Geotextiles and Geomembranes 29 (2010) 83–91

Contents lists available at ScienceDirect

Geotextiles and Geomembranes

journal homepage: www.elsevier.com/locate/geotexmem

Numerical analysis of tensile behavior of geogrids with rectangular and triangular apertures

Yan-Li Dong [a,b], Jie Han [b,*], Xiao-Hong Bai [a]

[a] College of Architecture and Civil Engineering, Taiyuan University of Technology, Taiyuan 030024, PR China
[b] Department of Civil, Environmental, and Architectural Engineering, the University of Kansas, Lawrence, KS 66045, USA

ARTICLE INFO

Article history:
Received 12 December 2009
Received in revised form
5 September 2010
Accepted 16 October 2010
Available online xxx

Keywords:
Geogrid
Polymeric material
Tensile behavior
Stress–strain relation
Triangular aperture

ABSTRACT

Geogrids, made of polymeric materials, have been used as a construction material for many applications, such as walls, slopes, roads, building foundations, etc. In the past, geogrids were manufactured with apertures in a rectangular or square shape. Recently, geogrids with a triangular aperture shape have been introduced into the market. The new geogrids are manufactured with ribs oriented in three equilateral directions and expected to have a more stable grid structure, which can provide more uniform resistance in all directions. In this study, the numerical software – FLAC was adopted to investigate the responses of geogrids with rectangular and triangular apertures when subjected to a uniaxial tensile load at different directions relative to the orientations of ribs in air. The geogrid ribs were modeled using beam elements jointed rigidly at nodes (i.e., the angle between two adjacent ribs did not change) and subjected to tension in one direction. The numerical results showed that the stress–strain responses of the geogrids were different at different loading directions relative to the orientations of ribs. The effects of aperture shape of geogrid, and elastic modulus and cross-section area of geogrid ribs on the tensile stiffness of the geogrid were also evaluated. The geogrid with triangular apertures had more uniform tensile stiffness and strength distributions than the geogrid with rectangular apertures. An increase of the elastic modulus and cross-section area of the geogrid ribs could increase the stiffness of the geogrid with triangular apertures. The numerical results were verified by experimental data for geogrids with rectangular and triangular apertures.

1. Introduction

Geogrids are made of polymeric materials (mostly high-density polyethylene, polypropylene, or polyester) with a different manufacturing process (extruded and punched-drawn, knitting, or welding). Details of the geogrid manufacturing can be found in the textbook by Koerner (2005). The geogrid manufactured by the extruded and punched-drawn process is unitized and has rigid joints at nodes (i.e., the angle between two adjacent ribs does not change during loading) due to much larger thickness at nodes than ribs. The extruded and punched-drawn geogrids will be investigated in this study. In the past, geogrids were manufactured with apertures in a rectangular or square shape. They are used to carry tensile force in one or two directions along the ribs. The geogrid with one-directional tensile strength is commonly referred to as uniaxial geogrid, which is mainly used for walls and slopes (for example, Han and Leshchinsky, 2010). The geogrid with two-directional tensile strengths is commonly referred to as biaxial geogrid, which is mainly used for roads, foundations, and pile-supported embankments. The use of geogrids has been increasing steadily over the past 30 years and is expected to continue to rise.

Recently, geogrids with a triangular aperture shape have been introduced into the market. The new geogrids are manufactured with ribs oriented in three equilateral directions and expected to have a more stable grid structure, which can provide more uniform resistance in all directions. The geogrid with triangular apertures is expected to be used in the similar applications as biaxial geogrids especially when the loading is not only in two directions. Fig. 1 shows the products of the geogrids with rectangular and triangular apertures.

The uses of biaxial geogrids for subgrade improvement, base and ballast reinforcement, foundation reinforcement, and pile-supported embankments have been studied by many researchers, for example,

* Corresponding author. Department of Civil, Environmental, and Architectural Engineering, the University of Kansas, 2150 Learned Hall, 1530 W, 15th Street, Lawrence, KS 66045-7609, USA. Tel.: +1 785 864 3714; fax: +1 785 864 5631.
E-mail addresses: qianxinjie@yahoo.com (Y.-L. Dong), jiehan@ku.edu (J. Han), bxhong@tyut.edu.cn (X.-H. Bai).

0266-1144/$ – see front matter © 2010 Elsevier Ltd. All rights reserved.
doi:10.1016/j.geotexmem.2010.10.007

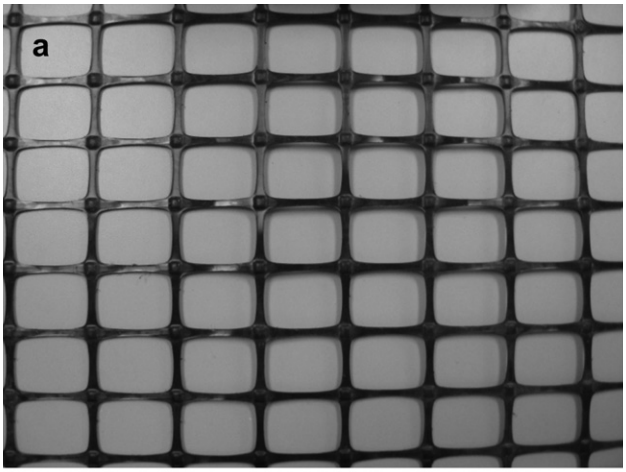

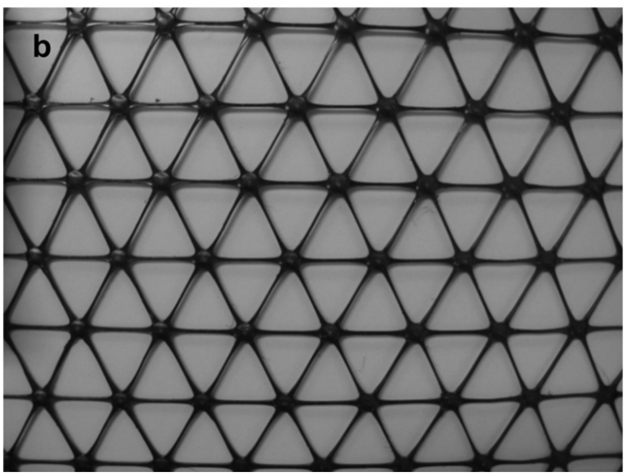

Fig. 1. Extruded and punched-drawn products of geogrids with rectangular and triangular apertures. (a) Geogrid with rectangular apertures, (b) Geogrid with triangular apertures.

Abdullah and Edil (2007), Adams and Collin (1997), Brown et al. (2007), Gailer (1987), Han and Akins (2002), Helstrom et al. (2006), Huang and Han (2009), Kinney et al. (1998), and Tang et al. (2008). Also, the behavior of biaxial geogrid-reinforced earth structures has been studied through field full-scale tests, laboratory model tests, and numerical simulation, for example, Abu-Farsakh et al. (2008), Sugimoto and Alagiyawanna (2003), and Viswanadham and KÖnig (2004). Guido et al. (1987) and DeMerchant et al. (2002) conducted a series of plate load tests to study the effects of several factors on the bearing capacity and stiffness of biaxial geogrid-reinforced aggregate beds. Gabr and Hart (2000) reported several model tests on biaxial geogrid-reinforced sand in terms of their elastic moduli. Giroud and Han (2004a, 2004b) presented a design method for biaxial geogrid-reinforced unpaved roads. Dong et al. (2010a) conducted a numerical investigation into the stress–strain responses of biaxial geogrids under uniaxial tension at different directions relative to the orientations of ribs. This study demonstrated the non-uniform distributions of tensile stiffness and strength of the biaxial geogrids for a specific geogrid product. Additional analyses were conducted in this study for biaxial geogrids.

The new geogrid products with triangular apertures recently introduced into the market are expected to have a more stable grid structure, which can provide more uniform resistance in all directions. However, limited test data related to the geogrids with triangular apertures have been published so far. Dong et al. (2010b) conducted six plate load tests to study the influence of the depth and type of the geogrids with triangular apertures on the reinforced sand bases. The effects of aperture shape, depth, and number of geogrids on the bearing capacity were investigated by Dong et al. (2010c). Dong et al. (2010c) found that the geogrid with triangular apertures was more efficient than that with rectangular apertures in terms of the ratio of the ultimate bearing capacity to the mass of the geogrid.

In this study, a numerical method was adopted to investigate the behavior of the geogrids with triangular apertures under uniaxial loading at different loading direction relative to the orientation of ribs. The reason for selecting a uniaxial loading test is that this test is the most common method to evaluate the stress–strain behavior of geosynthetics. In field, geosynthetics may be subjected to biaxial or multi-axial loading. The study on biaxial loading of geogrids is under way and will be presented in a future publication. The biaxial geogrid was also modeled for the comparison purpose. To be consistent with the terminology of the geogrid with triangular apertures, the term "geogrid with rectangular apertures" is used hereafter in this paper instead of the "biaxial geogrid". This paper presents the effect of the loading direction relative to the orientation of ribs on the stress–strain responses of the geogrids with rectangular and triangular apertures. In addition to the loading direction, this study studied the influence of the following factors on the tensile stiffness of the geogrids: aperture shape of geogrid, and elastic modulus and cross-section area of geogrid ribs.

2. Numerical modeling

The finite difference software – FLAC (Fast Lagrangian Analysis of Continua) 2D program Version 5.0 was adopted in this study to investigate the behavior of the geogrids with rectangular and triangular apertures under tension at different directions relative to the orientation of ribs. FLAC 2D has been successfully used by many researchers to study geotechnical problems, for example, Han and Gabr (2002) and Huang et al. (2009). Han and Gabr (2002) numerically investigated geosynthetic-reinforced fill platforms over pile foundations. In the Han and Gabr (2002) study, the geosynthetic reinforcement was modeled using solid elements. Huang et al. (2009) studied geosynthetic-reinforced column-supported embankments over soft soil using mechanically and hydraulically coupled models. In the Huang et al. (2009) study, the geosynthetic reinforcement was modeled using cable elements. FLAC models materials using solid elements in zones and/or structures elements in segments. The numerical results can include stresses and strains in each zone, displacements on each node, and axial force in each element, etc.

2.1. Model considerations

Beam elements, which can have bending stiffness and rigid connections at nodes, were used in this study to represent extruded and punched-drawn geogrids. Beam elements were jointed rigidly at nodes (i.e., the angle between two adjacent ribs at each node was maintained the same during the tensile test) to form apertures and a geogrid sheet. All the ribs were modeled as a linearly elastic-perfectly plastic material. Considering possible large deformation of a geogrid sample, a large-strain mode was chosen for the analysis.

To model a geogrid sample subjected to a uniaxial tensile load at a different direction relative to the orientation of ribs, the geogrid sheet was rotated around a fixed centroid to a desired angle (0, 45, 60, and 90°), cut into the dimension required for a wide width tensile test, and then subjected to a horizontal uniaxial tensile force. Based on ASTM D6637-01, the minimum size of the geogrid

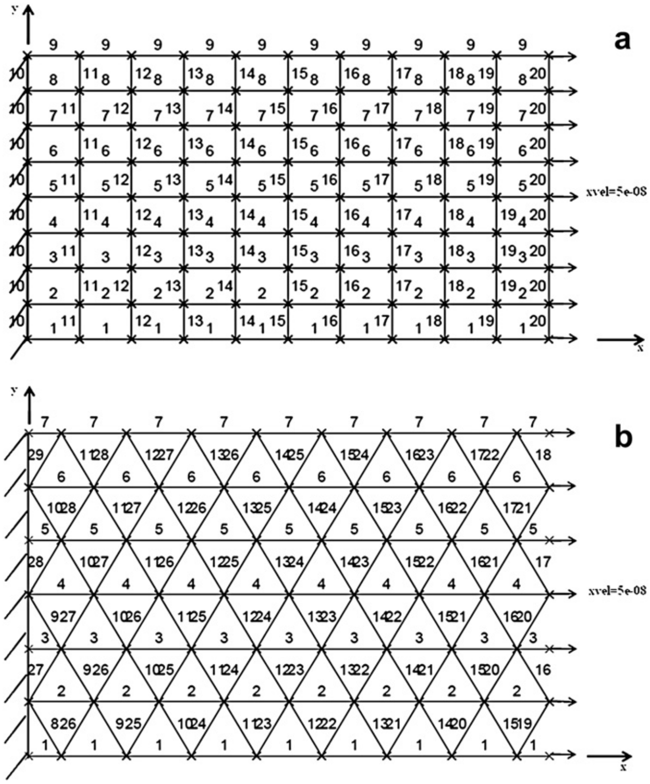

Fig. 2. Meshes with beam element numbers. (a) Geogrid with rectangular apertures, (b) Geogrid with triangular apertures.

specimen used in a tensile test should have a dimension of 300 mm long and 200 mm wide.

To simulate a tensile test in a laboratory, the mesh was fixed for movement in *x* and *y* directions and rotation at the left boundary and had a mesh size of 330 mm by 200 mm for a geogrid with rectangular apertures and 320 mm by 208 mm for a geogrid with triangular apertures, respectively, as shown in Fig. 2. The actual sample size larger than the minimum size of 300 mm × 200 mm required by ASTM D6637-01 was to accommodate complete apertures. Fig. 2(a) shows the numerical mesh for the geogrid with rectangular apertures oriented in a 0° angle (i.e., the cross-machine direction (XMD) of the geogrid) as an example. The reason for selecting the XMD as the 0° angle is that geogrids with rectangular and triangular apertures both have vertical ribs in the XMD. Fig. 2(b) shows the numerical mesh for the geogrid with triangular apertures oriented in a 0° angle as an example. The aperture sizes for both geogrids were selected based on real products in the market. The initial numbers of beam elements and nodes for these geogrids in the 0° angle are 178 and 99 for the geogrid with rectangular apertures and 67 and 102 for the geogrid with triangular apertures, respectively. The analyses of the behavior of these two products will be presented in the following section. The numbers appearing in Fig. 2 are the beam element numbers used in the numerical analysis. An equal velocity at 5 e^{-8} m/step was applied horizontally on each node on the right boundary with an increasing magnitude until the failure of the sample. The right boundary could only move in the x direction but not in the *y* direction. The right boundary did not allow any rotation either. This boundary was created to simulate a clamp in a laboratory test. The top and bottom boundaries of these meshes were free for displacements in the *x* and *y* directions.

Table 1
Index properties of biaxial geogrids.

Parameters	Units	Real		Simplified
		MD	XMD	MD/XMD
Aperture dimensions	mm	25	33	25/33
Rib thickness	mm	1.27	1.27	1.27
Rib width	mm	3	3	3
Tensile stress @ 2% strain	kN/m	6.0	9.0	9.0
Ultimate tensile strength	kN/m	19.2	28.8	28.8

2.2. *Model verification*

To verify the numerical model, an extruded and punched-drawn geogrid with rectangular apertures available in the market was selected for this purpose. The index properties of this geogrid from the manufacturer are provided in Table 1. The elastic moduli and yield strengths of the beam elements used in the FLAC software were determined based on the tensile stresses at 2% strain and the ultimate strengths in the machine and cross-machine directions, respectively, in Table 1. Fig. 3 shows the numerical results compared with the test data for the real geogrid with rectangular apertures listed in Table 1. The comparison shows reasonable agreement for the tensile stiffness (i.e., the initial slope) and the ultimate tensile strength (i.e., the horizontal line) in both XMD (0° direction) and MD (90° direction) between the numerical and experimental results. The horizontal lines in Fig. 3 and later figures represent the maximum (peak) loads a geogrid can carry. The geogrid may continue carrying a load after reaching this maximum load, but at a reduced magnitude. The tensile stiffness and the ultimate tensile strength are two key parameters from tensile tests and used in the design; therefore, they are also the focuses of this study. The after-peak stress–strain behavior is not the focus of this study. It is expected that the linearly elastic-perfectly plastic model cannot simulate the nonlinear behavior of the geogrid material. It is also worth pointing out that the yield strain for the geogrid ribs was at 6.4%. Detailed discussion on this verification can be found in Dong et al. (2010a).

3. Numerical results and analysis

3.1. *Rectangular aperture geogrids with different properties*

The real geogrid product with rectangular apertures discussed above has different tensile stiffness and strength values in MD and

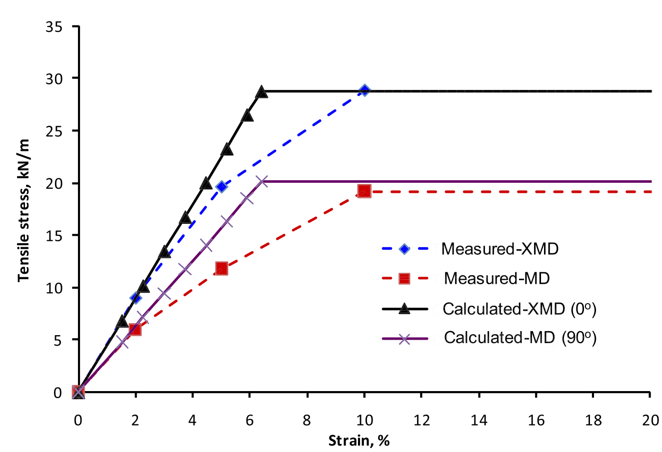

Fig. 3. Numerical and test results of geogrid with rectangular apertures subjected to tensile force at 0° and 90° (Dong et al., 2010a).

Please cite this article in press as: Dong, Y.-L., et al., Numerical analysis of tensile behavior of geogrids with rectangular and triangular apertures, Geotextiles and Geomembranes (2010), doi:10.1016/j.geotexmem.2010.10.007

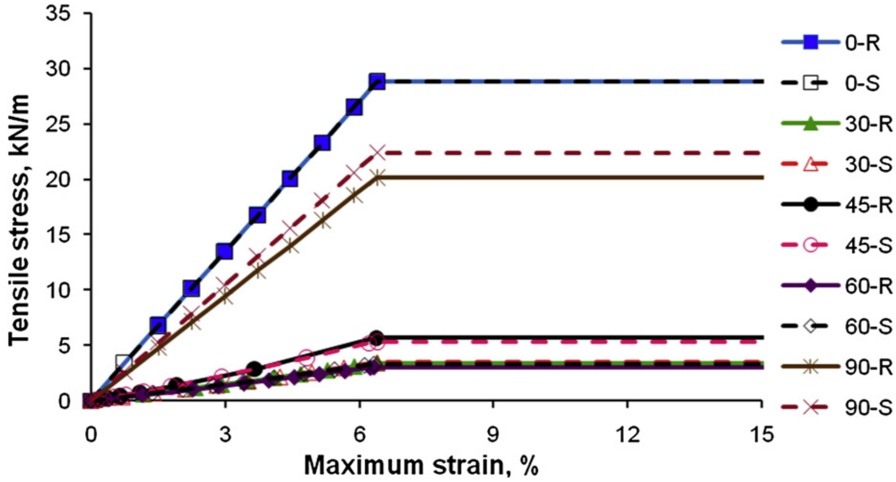

Fig. 4. Computed stress–strain responses of real and simplified geogrids with rectangular apertures based on maximum strains in ribs.

XMD. As a result, the ribs in MD and XMD for this product have different tensile stiffness and strength values. To investigate the effect of the tensile stiffness and strength and be easier for the comparison with the triangular aperture geogrids, a simplified rectangular aperture geogrid with equal rib tensile stiffness and strength values in MD and XMD was selected and analyzed in this study. The properties of the simplified properties are provided in Table 1.

Figs. 4 and 5 present the numerical results based on the real product properties as compared with the simplified product properties. R in the figures represents the real geogrid product while S represents the simplified geogrid product. For the simplified geogrid, it had the same material properties in both MD and XMD as those in XMD for the real geogrid. It is shown that the numerical results of the stress–strain responses of the geogrids subjected to 0–90° loading relative to the orientation of XMD ribs using the simplified properties matched those using the real properties of geogrid reasonably well except those at a 90° loading. It is understandable that the simplified geogrid had higher tensile stiffness and strength at the 90° loading than the real geogrid as shown in Table 1. Therefore, the numerical results of the simplified geogrid with rectangular apertures will be compared with those of the geogrid with triangular apertures. The maximum strain in Fig. 4 is the largest strain developed among all the ribs in each geogrid sample. However, the average strain of the sample could be calculated by the horizontal displacement at the right boundary divided by the initial length of the sample. As shown in Figs. 4 and 5, significant differences in the strain values, if the maximum or average strain is used, exist for the geogrids subjected to a 45° loading relative to the orientation of XMD ribs. As observed by Dong et al. (2010a) and also shown later in this paper, the geogrid developed significant necking at a 45° loading. Minor differences in the strain values for the geogrids at other directional loading are observed.

3.2. Geogrids with rectangular versus triangular apertures

All the geogrid ribs were first modeled used the same tensile stiffness and strength and rib cross-section area for both geogrids with rectangular (33 × 25 mm) and triangular (40 × 40 × 40 mm) apertures to evaluate the effect of the aperture shape. Then, a parametric study was conducted to evaluate the effect of the elastic modulus and the cross-section area of the ribs. The geogrid with rectangular apertures is designated as Geogrid B while the geogrids with triangular apertures are designated as Geogrids T1, T2, and T3, respectively. The parameters used for this numerical study are provided in Table 2. Geogrid T1 had the same elastic

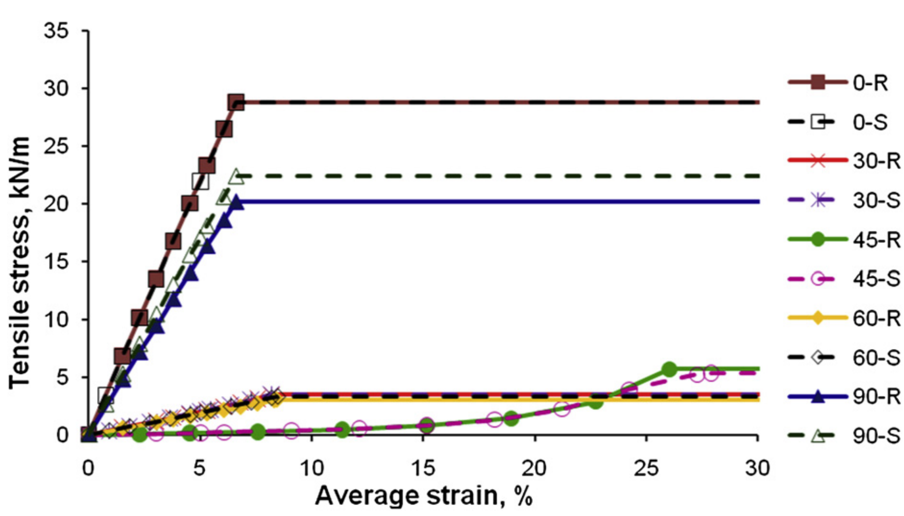

Fig. 5. Computed stress–strain responses of real and simplified geogrids with rectangular apertures based on average strains of sheets.

Please cite this article in press as: Dong, Y.-L., et al., Numerical analysis of tensile behavior of geogrids with rectangular and triangular apertures, Geotextiles and Geomembranes (2010), doi:10.1016/j.geotexmem.2010.10.007

Table 2
Rib properties used for numerical analysis.

Type	Elastic modulus (GPa)	Cross-section area ($\times 10^{-6}$ m^2)	Moment of inertia ($\times 10^{-12}$ m^4)	Yield strength (MPa)
B	2.625	3.81	0.512	168
T1	2.625	3.81	0.512	168
T2	6.552	3.81	0.512	168
T3	6.552	1.95	0.366	168

modulus, tensile strength, and rib cross-section area as Geogrid B. Geogrid T2 had the same tensile strength and rib cross-section area as Geogrid T1 but had 2.5 times elastic modulus as Geogrid T1. Geogrids T1 and T2 were used to investigate the effect of the elastic modulus of geogrid ribs on the behavior of the geogrids with triangular apertures. Geogrid T3 had material properties similar to one product available in the market and had half of the rib cross-section area as Geogrid T2. Geogrids T2 and T3 were used to investigate the effect of the rib cross-section area on the behavior of the geogrids with triangular apertures.

3.2.1. Strain in geogrid under uniaxial tension

Figs. 6 to 10 present the strain distributions in the ribs (i.e., beam elements) of Geogrids B and T1 at the beginning of rib yielding (i.e., $\varepsilon_{max} = 6.4\%$) under uniaxial tension at different loading directions to the orientation of the XMD ribs. Fig. 6 shows the strain distributions of the geogrids with rectangular and triangular apertures under 0° tension (i.e., same as the XMD), in which a uniform strain distribution developed in the ribs at the same direction as the loading. For the geogrid with rectangular apertures, there was nearly zero strain in the ribs at the direction perpendicular to the loading. For the geogrid with triangular apertures, smaller strains developed at the longitudinal and diagonal directions especially near the right and left boundaries. Slight necking is observed in the geogrid with triangular apertures.

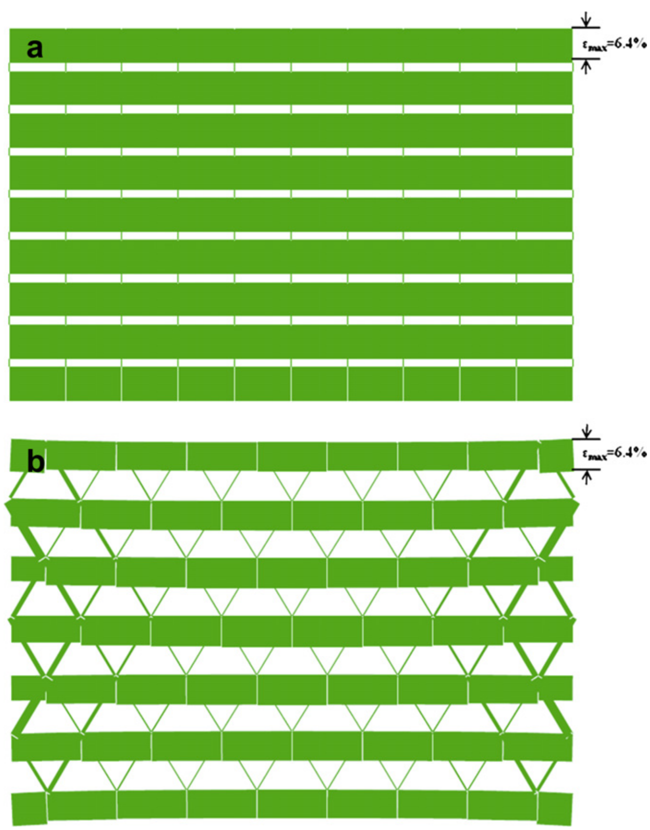

Fig. 6. Strain distributions in ribs under 0° tension. (a) Geogrid with rectangular apertures, (b) Geogrid with triangular apertures.

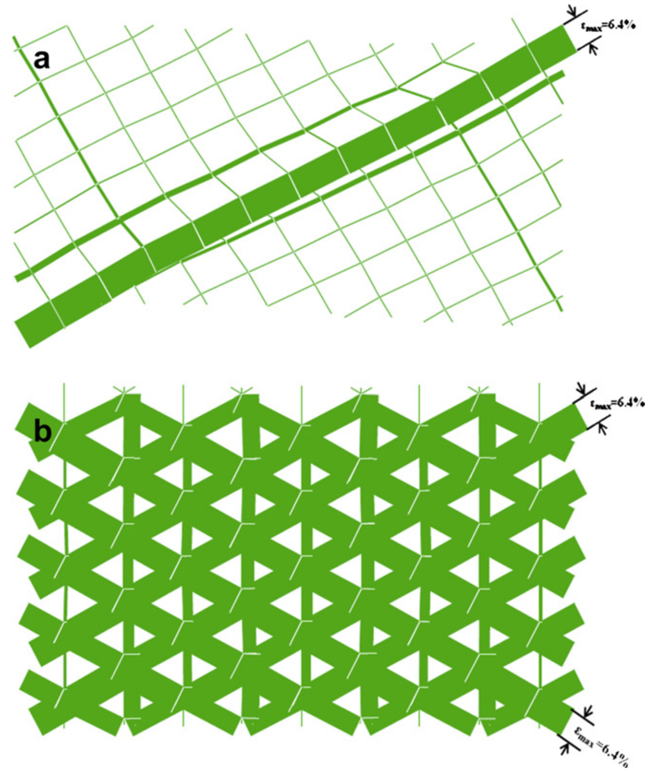

Fig. 7. Strain distributions in ribs under 30° tension. (a) Geogrid with rectangular apertures, (b) Geogrid with triangular apertures.

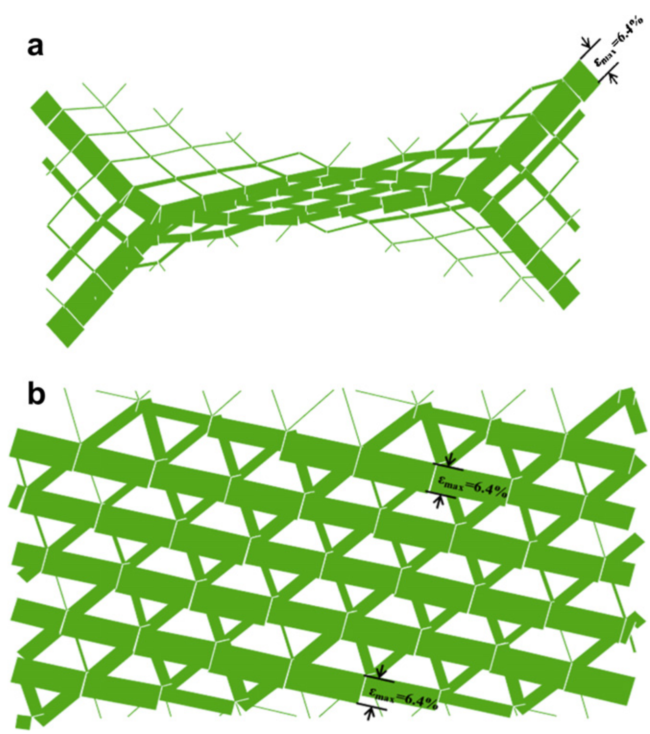

Fig. 8. Strain distributions in ribs under 45° tension. (a) Geogrid with rectangular apertures, (b) Geogrid with triangular apertures.

Please cite this article in press as: Dong, Y.-L., et al., Numerical analysis of tensile behavior of geogrids with rectangular and triangular apertures, Geotextiles and Geomembranes (2010), doi:10.1016/j.geotexmem.2010.10.007

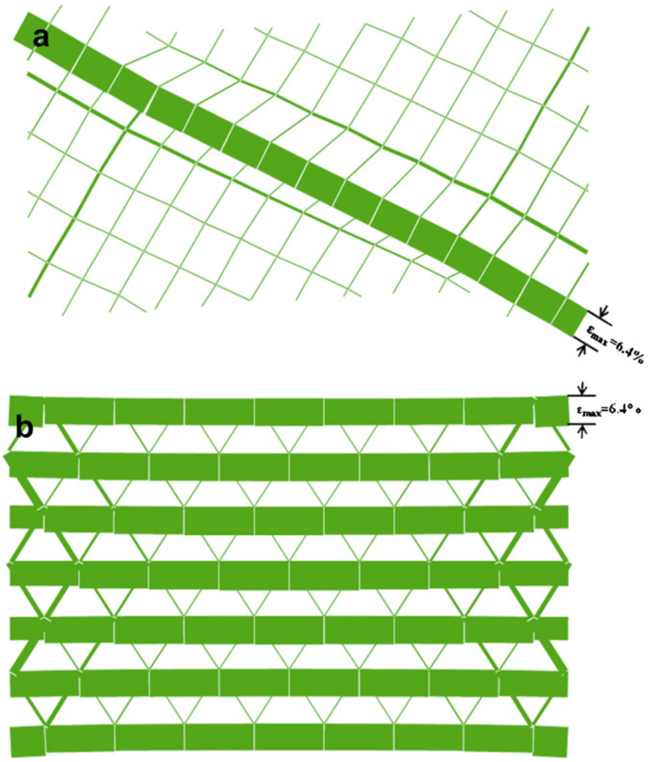

Fig. 9. Strain distributions in ribs under 60° tension. (a) Geogrid with rectangular apertures, (b) Geogrid with triangular apertures.

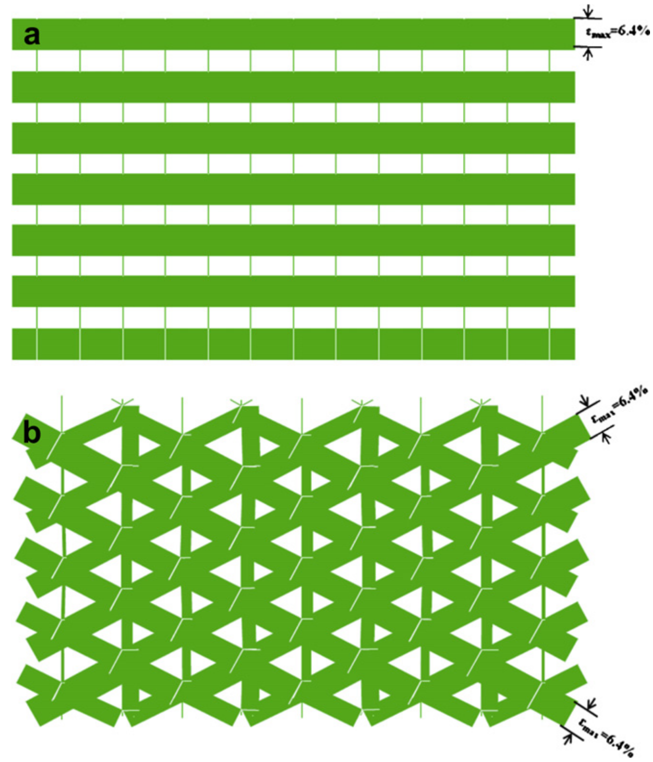

Fig. 10. Strain distributions in ribs under 90° tension. (a) Geogrid with rectangular apertures, (b) Geogrid with triangular apertures.

Fig. 7 shows the strain distributions in the ribs of both geogrids subjected to 30° tension. For the geogrid with rectangular apertures, higher strains only concentrated along the diagonal rib. For the geogrid with triangular apertures, relatively uniform strains developed in all the ribs even though the ribs oriented in the vertical direction had lower strains than other two directions.

Fig. 8 shows the deformed geogrids and the strain distributions in the ribs under tension at the 45° angle to the loading direction. The geogrid with rectangular apertures had obvious necking with excessive extension in the loading direction. However, the geogrid with triangular apertures had relatively uniform strains in all the ribs without any obvious necking. Since the orientations of the ribs of the geogrid with rectangular aperture are symmetric to the loading direction at 45°, the strain distributions in this geogrid are also symmetric.

Fig. 9 shows the strain distributions in the ribs under tension at the 60° angle to the loading direction. It is shown that the numerical results for the geogrid with rectangular apertures are almost the same as those at the 30° angle in Fig. 7(a) while the numerical results for the geogrid with triangular apertures are the same as those at the 0° angle in Fig. 6(b). These similarities resulted from the orientations of the ribs.

Fig. 10 presents the strain distributions of both geogrids under 90° tension. It is shown that the geogrid with rectangular apertures had a uniform strain distribution in the ribs at the same direction to the tension but had nearly zero strain in the ribs at the direction perpendicular to the tension. However, the geogrid with triangular apertures had relatively uniform strain distributions in all the ribs even though the ribs oriented in the vertical direction had relatively lower strains.

The numerical results showed that the geogrid with rectangular apertures subjected to the tension at the direction different from 0 (XMD) and 90 (MD) degrees deformed more extensively than the geogrid with triangular apertures. The above discussion demonstrated that the strains in the geogrids with triangular apertures were more uniformly distributed than the geogrids with rectangular apertures in all the loading directions. In other words, the geogrid with triangular apertures is more effective and efficient than that with rectangular apertures in resisting tensile force at the directions different from the orientations (i.e., MD and XMD) of the ribs.

3.2.2. Stress–strain curve

Fig. 11 shows the stress–strain curves of two geogrids, B and T1, under uniaxial tension at the directions from 0° to 90° relative to the XMD ribs. The curves are plotted in two ways: (1) using the maximum strain of the geogrid ribs at yield (i.e., Fig. 11(a)) and (2) using the average strain (i.e., Fig. 11(b)). Except for Geogrid B at 45° loading, the stress–strain curves for both geogrids at other directions of loading are the same based on either the maximum strain or the average strain. As shown in Fig. 11, Geogrid B at 45° loading started to carry the load after having the strain more than 15% because of necking. Fig. 11 shows that Geogrid B at the 0° loading had the highest tensile strength because there were more ribs in this direction than that in the 90° loading. Although the highest tensile strength of Geogrid T1 was lower than that of Geogrid B, Geogrid T1 had a more uniform tensile strength distribution than Geogrid B. This result can be seen even more clearly in Fig. 12. Figs. 11 and 12 both show that the geogrids with triangular apertures had the same tensile strength values at 0 and 60° loadings and 30 and 90° loadings, respectively. However, the tensile strengths at the 30 and 90° loadings were slightly higher than those at the 0 and 60° loadings.

3.2.3. Tensile stiffness distributions

A parametric study was conducted to investigate the effect on the tensile stiffness distributions by three influence factors: (1)

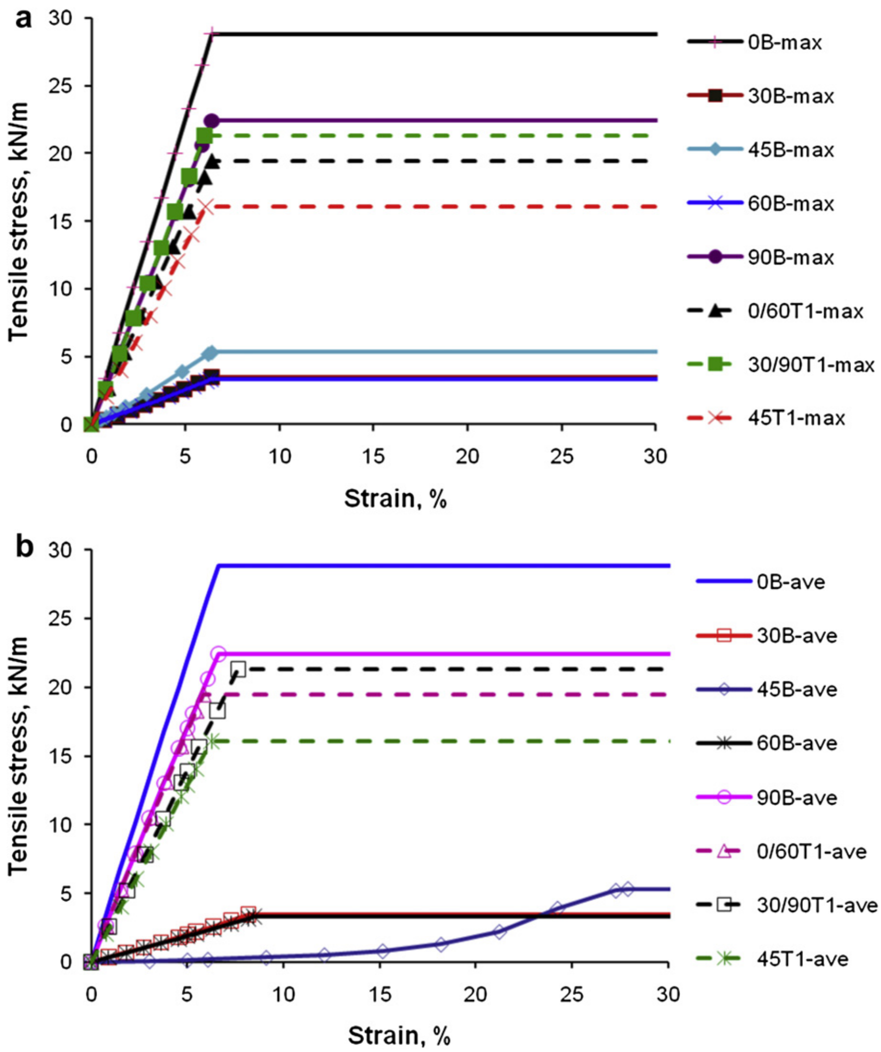

Fig. 11. Stress–strain curves of geogrid with rectangular and triangular apertures at all loading directions. (a) Maximum strain, (b) Average strain.

aperture shape, (2) elastic modulus of ribs, and (3) cross-section area of ribs.

Fig. 13 shows the tensile stiffness distributions of Geogrids B and T1. The tensile stiffness for the geogrids at all directions was determined at 5% average strain, which is typically used in practice. As shown in Fig. 11, the tensile stiffness (i.e., the initial slope) is constant from 0 to 6.4% for each geogrid at a certain loading direction except Geogrid B at a 45° loading. Fig. 13 shows that the tensile stiffness of Geogrid B is highly dependent on the loading direction relative to the orientation of ribs while that of Geogrid T1 is relatively uniformly distributed. At 0 and 90° loadings, Geogrid B had higher tensile stiffness but much lower tensile stiffness at other

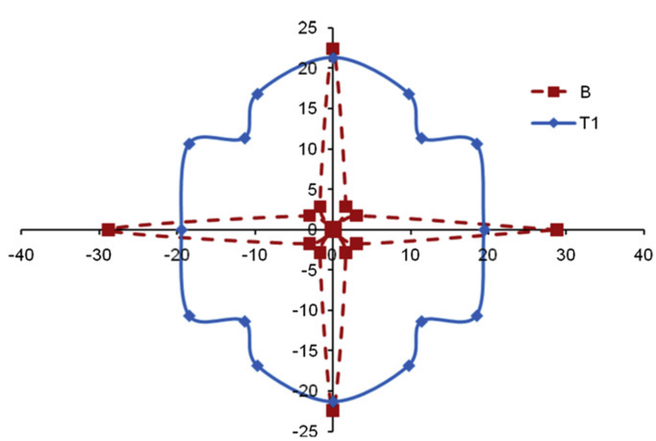

Fig. 12. Distribution of tensile strengths around 360° (unit: kN/m).

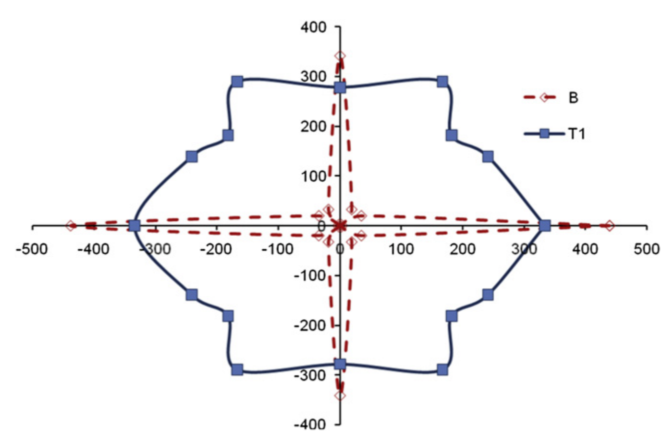

Fig. 13. Tensile stiffness of geogrids with different aperture shapes around 360° (units: kN/m).

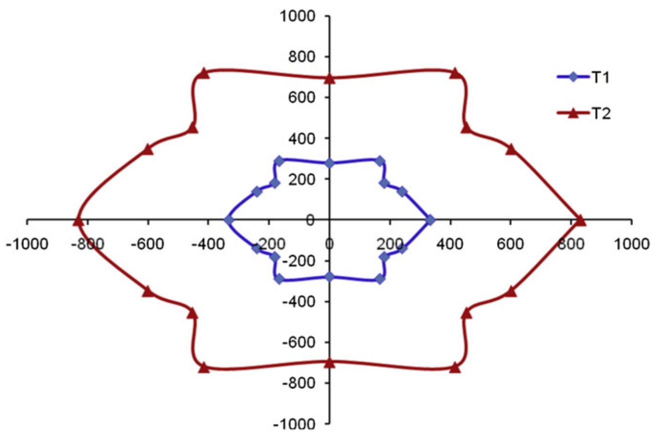

Fig. 14. Tensile stiffness of geogrids with different rib moduli around 360° (units: kN/m).

Directional loadings. The lowest tensile stiffness of Geogrid B was at the 45° loading relative to the orientation of XMD ribs. For Geogrid T1, the higher tensile stiffness was at the three principal directions of ribs and that at other directions was slightly lower. It is also true that the lowest tensile stiffness for Geogrid T1 was at the 45° loading.

To investigate the effect of rib elastic modulus on the tensile stiffness of geogrids with triangular apertures, numerical analyses were performed for two geogrids (T1 and T2) with different rib elastic moduli. Fig. 14 presents the numerical results of the tensile stiffness of the geogrids with different rib elastic moduli. It is shown that an increase of the elastic modulus of the ribs increased the tensile stiffness of the geogrid.

Numerical analyses were also conducted to study the effect of rib cross-section area on the tensile stiffness of the geogrid with triangular apertures. Fig. 15 shows that an increase of the cross-section area of ribs increased the tensile stiffness of the geogrid. Of course, an increase in the cross-section area of ribs would increase the amount of polymeric materials used to manufacture the geogrid and thus increase the cost. The distribution of the measured tensile stiffness of one geogrid with triangular apertures obtained independently by SGI Testing Services (2010) is included in Fig. 15. This geogrid had similar material properties as Geogrid T3. It is shown that the measured distribution matches the computed one of Geogrid T3 very well. More importantly, the measured result confirms the shape of the tensile stiffness distribution of the geogrid with triangular apertures. This comparison demonstrates the reasonableness of the numerical results.

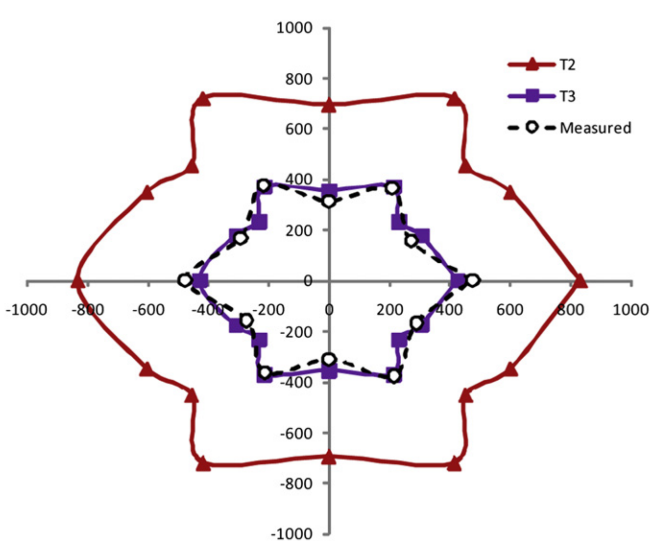

Fig. 15. Tensile stiffness of geogrids with different rib cross-section areas around 360° (units: kN/m).

4. Conclusions

The tensile behavior of geogrids with rectangular and triangular apertures under uniaxial tension at different directions relative to the orientation of ribs was investigated using the numerical software – FLAC. Based on this numerical analysis, the following conclusions can be made:

(1) The tensile strength and stiffness of the geogrid with rectangular apertures were highly dependent on the direction of the uniaxial tension relative to the orientation of ribs. When the tension was applied in the same direction as the rib orientation, either machine or cross-machine direction, the tensile strength and stiffness were high. At other directions, they were much lower. The tensile strength and stiffness of the geogrid at a 45° loading were lowest, which were nearly zero.
(2) The tensile strength and stiffness of the geogrid with triangular apertures were relatively uniform at all the loading directions relative to the orientation of ribs even though those at the 45° loading were slightly lower. This study confirmed that the geogrid with triangular apertures has much more uniform stress and strain distributions among the ribs than the geogrid with rectangular apertures. Therefore, the geogrid with triangular apertures is more effective and efficient to carry uniaxial tension from different directions than the geogrid with rectangular apertures.
(3) An increase of the elastic modulus and/or cross-sectional area of ribs increased the tensile stiffness of the geogrid with triangular apertures.
(4) The experimental data matches the numerical results of geogrids with rectangular and triangular apertures well and verifies the reasonableness of the numerical method.

Acknowledgement

The first author was sponsored by the Chinese Scholarship Council to be a visiting scholar at the University of Kansas in the United States. This sponsorship is greatly appreciated.

References

Abdullah, C.H., Edil, T.B., 2007. Behavior of geogrid-reinforced load transfer platforms for embankment on rammed aggregate piers. Geosynthetics International 14 (3), pp. 141–153.
Abu-Farsakh, M., Chen, Q.M., Sharma, R., Zhang, X., 2008. Large-scale model footing tests on geogrid-reinforced foundation and marginal embankment soils. Geotechnical Testing Journal 31 (5), pp. 413–423.
Adams, M.T., Collin, J.G., 1997. Large model spread footing load tests on geosynthetic reinforced soil foundations. Journal of Geotechnical and Geoenvironmental Engineering 123 (1), pp. 66–72. ASCE.
Brown, S.F., Kwan, J., Thom, N.H., 2007. Identifying the key parameters that influence geogrid reinforcement of railway ballast. Geotextiles and Geomembranes 25 (6), pp. 326–335.
DeMerchant, M.R., Valsangkar, A.J., Schriver, A.B., 2002. Plate load tests on geogrid-reinforced expanded shale lightweight aggregate. Geotextiles and Geomembranes 20 (3), pp. 173–190.
Dong, Y.L., Han, J., Bai, X.H., 2010a. A numerical study on stress-strain responses of biaxial geogrids under tension at different directions. In: Proceedings of ASCE Geo-Institute GeoFlorida 2010, West Palm Beach, Florida, February 20 to 24, Advances in Analysis, Modeling & Design. Geotechnical Special Publication No. 199, pp. 2551–2560.
Dong, Y.L., Han, J., Bai, X.H., 2010b. Behavior of triaxial geogrid-reinforced bases under static loading. Geosynthetics for A Challenging World. In: Palmeira, E.M.,

Vidal, D.M., Sayao, A.S.J.F., Ehrlich, M. (eds.), Proceedings of the 9th International Conference on Geosynthetics, May 23–27, 2010. Brazil, pp. 1547–1550.

Dong, Y.L., Han, J., Bai, X.H., 2010c. Bearing capacities of geogrid-reinforced sand bases under static loading. Ground Improvement and Geosynthetics. Geotechnical Special Publication No. 207. In: Puppala, A.J., Huang, J., Han, J., Hoyos, L.R. (eds.), Proceedings of the GeoShanghai International Conference, June 3 to 5, 2010. Shanghai, China, pp. 275–281.

Gabr, M.A., Hart, J.H., 2000. Elastic modulus of geogrid-reinforced sand using plate load tests. Geotechnical Testing Journal 23 (2), pp. 245–250.

Gailer, J.E., 1987. Geogrids working on the railroad. Railway Track and Structures 83 (6), 32–34.

Giroud, J.P., Han, J., 2004a. Design method for geogrid-reinforced unpaved roads: I. Development of design method. Journal of Geotechnical and Geoenvironmental Engineering 130 (8), pp. 775–786. ASCE.

Giroud, J.P., Han, J., 2004b. Design method for geogrid-reinforced unpaved roads: II. Calibration and applications. Journal of Geotechnical and Geoenvironmental Engineering 130 (8), pp. 787–797. ASCE.

Guido, V.A., Knueppel, J.D., Sweeny, M.A., 1987. Plate Loading Tests on Geogrid-reinforced Earth Slabs. Geosynthetics 87 Conference, New Orleans, pp. 216–225.

Han, J., Akins, K., 2002. Use of geogrid-reinforced and pile-supported earth structures. Geotechnical Special Publication No.116-Deep Foundations 2002. In: O'Neill, M.W., Towsend, F.C. (Eds.), Proceedings of International Deep Foundation Congress. ASCE, Orlando, USA, pp. 668–679.

Han, J., Gabr, M.A., 2002. Numerical analysis of geosynthetic-reinforced and pile-supported earth platforms over soft soil. Journal of Geotechnical and Geoenvironmental Engineering 128 (1), pp. 44–53. ASCE.

Han, J., Leshchinsky, D., 2010. Analysis of back-to-back mechanically stabilized earth walls. *Geotextiles and Geomembranes* 28 (3), pp. 262–267.

Helstrom, C.L., Humphrey, D.N., Hayden, S.A., 2006. Geogrid reinforced pavement structure in a cold region. In: Proceedings of 13th International Conference on Cold Regions Engineering: Current Practices in Cold Regions Engineering. Orono, ME, USA, pp. 57–69.

Huang, J., Han, J., 2009. 3D coupled mechanical and hydraulic modeling of a geosynthetic-reinforced deep-mixed column-supported embankment. Geotextiles and Geomembranes 27, pp. 272–280.

Huang, J., Han, J., Oztoprak, S., 2009. Coupled mechanical and hydraulic modeling of geosynthetic-reinforced column-supported embankments. Journal of Geotechnical and Geoenvironmental Engineering 135 (8), pp. 1011–1021. ASCE.

Kinney, T.C., Stone, D.K., Schuler, J., 1998. Using geogrids for base reinforcement as measured by falling weight deflectometer in full-scale laboratory study. Transportation Research Record 1611, pp. 70–77.

Koerner, R.M., 2005. Designing with Geosynthetics, fifth ed. Pearson Prentice Hall, pp. 796.

SGI Testing Services, 2010. Laboratory Test Results for Tensar TriAx Geogrids. Report to Tensar International Corporation.

Sugimoto, M., Alagiyawanna, A.M.N., 2003. Pullout behavior of geogrid by test and numerical analysis. Journal of Geotechnical and Geoenvironmental Engineering 129 (4), pp. 361–371. ASCE.

Tang, X.C., Chehab, G.R., Palomino, A., 2008. Evaluation of geogrids for stabilizing weak pavement subgrade. International Journal of Pavement Engineering 9 (6), pp. 413–429.

Viswanadham, B.V.S., KÖnig, D., 2004. Studies on scaling and instrumentation of a geogrid. Geotextiles and Geomembranes 22 (5), pp. 307–328.

Please cite this article in press as: Dong, Y.-L., et al., Numerical analysis of tensile behavior of geogrids with rectangular and triangular apertures, Geotextiles and Geomembranes (2010), doi:10.1016/j.geotexmem.2010.10.007